Bending waves focusing in arbitrary shaped plate-like structures: Study of temperature effects, development of a digital twin and of an associated neural-network based compensation procedure

Nassim Benbara [a,*], Guillaume Martin [b], Marc Rébillat [a], Nazih Mechbal [a]

[a] *Processes and Engineering in Mechanics and Materials laboratory (PIMM) ENSAM, CNRS, CNAM, HESAM Université, 151 Boulevard de l'Hôpital, 75013 Paris, France*
[b] *SDTools, 44 Rue Vergniaud, 75013, Paris, France*

Advanced automotive audio applications are more and more demanding with respect to the visual impact of loudspeakers while still requiring more and more channels for high quality spatial audio rendering. Removing classical heavy and large electrodynamic loudspeakers and using car interior plate-like structures driven by state of the art spatial sound algorithms appear as a promising solution to tackle both issues. However, to meet spatial audio rendering constraints, the bending waves generated within car interior plate-like structures must be focused at a given position and to a certain extent within the host structure. Theoretically, this means being able to invert in a robust manner the spatio-temporal wave propagation operator for the generated bending waves to fit a given target shape. The propagation operator inversion method considered here is the spatio-temporal inverse filtering (STIF) method based on the knowledge of the propagation operator on a regular spatial grid over the structure at a given temperature. However, in a car interior a high temperature variations exist and can adversely impact the performances of the STIF method, mainly because dynamical properties of the host structure (built up with polypropylene in most cases) largely vary within this temperature range. Even if the STIF method has already been adapted and assessed in the context of automotive audio reproduction, no study dealing with the effects of temperature on the STIF method and providing potential mitigation procedures avoiding experimental measurements at each temperature has been reported. To address that issue, the influence of temperature on the behavior of a polypropylene plate is first experimentally quantified. A model updating method is used to build a finite-element model of the plate taking into account temperature effects. This digital twin of the host-structure is then used to assess the influence of the temperature on the STIF method. A neural network based controller is finally trained and validated on the digital twin in order to compensate for the effects of temperature on STIF filters. Obtained results demonstrate that this procedure successfully allows to compensate for temperature effects on the STIF method applied to polypropylene plate with very limited experimental needs, thus paving the way through an industrial development of such approaches.

1. Introduction

Advanced automotive audio applications are more and more demanding with respect to the visual impact of loudspeakers while still requiring more and more channels for high quality spatial sound rendering. Removing classical heavy and large electrodynamic loudspeakers and using car interior plate-like structures driven by state of the art spatial sound rendering algorithms appear as an adequate solution to tackle both issues. Indeed, spatial sound rendering will allow to alert directionally the driver from several dangers and to provide passengers with higher quality spatial audio. This approach can also potentially decrease weight by replacing large and heavy electrodynamical loudspeakers with lighter piezoelectric elements or audio exciters. It can furthermore release some of the actual design constraints (electrodynamical loudspeakers placed at fixed positions and covered with grids for example) and provide car interior designers with new degrees of freedom. As a consequence, using spatial sound rendering coupled with flat panel loudspeaker appears as very appealing, particularly in the automotive industry.

The main idea behind the concept of spatial sound rendering algorithms is to calibrate each loudspeaker of the array to reproduce with high fidelity the physics and the acoustics of the primary source [1]. Historically, spatial rendering methods such as stereophony (virtual based amplitude panning: VBAP), binaural rendering or holophony (ambisonic or Wave Field Synthesis: WFS) have been achieved by means of electromagnetic loudspeakers. There are many constraints imposed by such methods for them to work properly: the setup must consist of several loudspeakers behaving like omnidirectional monopoles and with a flat and omnidirectional response that are spatially evenly distributed over the whole restitution area [2]. Even if electrodynamical loudspeakers have mainly been used for spatial audio rendering purposes, several alternative loudspeaker technologies have been proposed and among them planar loudspeakers. The idea behind planar loudspeakers is to produce sound waves by exciting the bending waves of a sufficiently thin and stiff plate through electrodynamical or piezoelectric actuators. A first attempt in that direction was the Distributed Mode Loudspeakers (DML) technology [3]. As DML were suffering from a poor response in the low frequency range, alternate technologies relying on multiple actuators (Multi-Actuator Panels [MAP]) or on much larger plates (Large Multi-Actuator Panels [LaMAP]) have been designed [4]. It consists in driving several audio exciters bonded on the MAP with different audio signals. Such technologies have been successfully used in the context of WFS [5,6] and thus have shown their ability to provide satisfying results for spatial audio rendering purposes. However, it still suffer from the modal behavior of the plate and the cross talk cancellation of the audio exciters. More recently, some references as [7,8] have studied the passive control of plates to improve their sound radiation.

In order to cope with spatial audio rendering algorithms constraints (omnidirectional loudspeakers with a flat frequency response) and to improve existing planar loudspeaker technologies, the idea of focusing bending waves on arbitrary plate-like structure to create independent sound sources appears as promising. This can allow to create an array of audio sources that can be used in a second time for spatial sound rendering. In the literature, there are various methods that allow to focus bending waves in a media. The first method called modal control (MC) is based on the modal superposition principle. It allows focusing an audio source on a rectangular plate by computing a set of 3 coefficient FIR filters [9]. The second method available in the literature is based on the time reversal (TR) principle, initially described by Fink et al. [10]. It allows to focus a wave at a specific point in the space by learning only the waves received at the actuator positions and initiated at the focusing point. The third method allowing to focus bending waves, and the one retained here, is the spatio-temporal inverse filtering (STIF), initially presented by [11] and [12] to find a solution to the lack of robustness of the time reversal method. The STIF method consists in experimentally learning the bending waves propagation operator in the whole media, and then to inverse it in order to design adequate focusing filters for each actuator. This method has been used in [13–15] with a plate actuated by exciters at the periphery to generate bending waves in the middle of the plate allowing to radiate a uniform sound field. The same authors also used this method to create a piston on a vehicle's roof for a narrow bass frequency band [16]. In [17], a study comparing the performances of the three previously mentioned bending wave focusing methods when varying several key parameters (such as geometrical complexity, host structure thickness and damping, number and location of actuators, and position and extent of the focusing area) has been conducted in order bridge the gap between previous academic studies and practical implementations of bending wave focusing algorithms.

As previously stated, automotive applications are targeted here and the temperature in a car interior can in practice vary over an extremely wide range (depending on the geographical area and the season) which can result in a wide effect on the material properties (stiffness, damping, etc...) of the host structure. The material used here is the polypropylene, because widely used in the automotive industry for garnishments. It has multiple advantages such as good recycling and durability properties. However, it is fragile at low temperatures and sensitive to UV radiations. Several articles demonstrated large variations of polypropylene [18,19], poly(butylene terephthalate) [20] and polymer [21] material properties with temperature. Consequently, performances of bending wave focusing algorithms are impacted by these large temperature changes as wave propagation within the host structure will be impacted by varying material properties. The effect of temperature on the host structure material properties (mainly polypropylene in car industry) and on the bending wave focusing algorithms must thus be understood and compensated for an effective and robust deployment of these solutions in the automotive context. In areas different from sound rendering but still involving propagating waves, several studies have been conducted to analyze the effect of temperature on structural dynamics in order to be able to compensate for these effects. In structural health monitoring of composite aeronautic structures, where Lamb waves are used to monitor potential damages in a structure, several temperature compensation methods have been proposed. In [22], the authors compensate the temperature effects through dynamic warping and stretch-based methods. Another approach assuming a compensation of a phase shift and amplitude factor induced by the temperature is proposed in [23]. Besides, the real time inspection of bridges in civil engineering is another important part of studies dealing with temperature compensation. The main issue is to establish a link between the structure eigenfrequencies and temperature for getting rid of the thermal, wind or moisture effects. Several methods use linear regressions [24], multilinear regression models (MLR) [25] and autoregressive model (ARMA) [26].
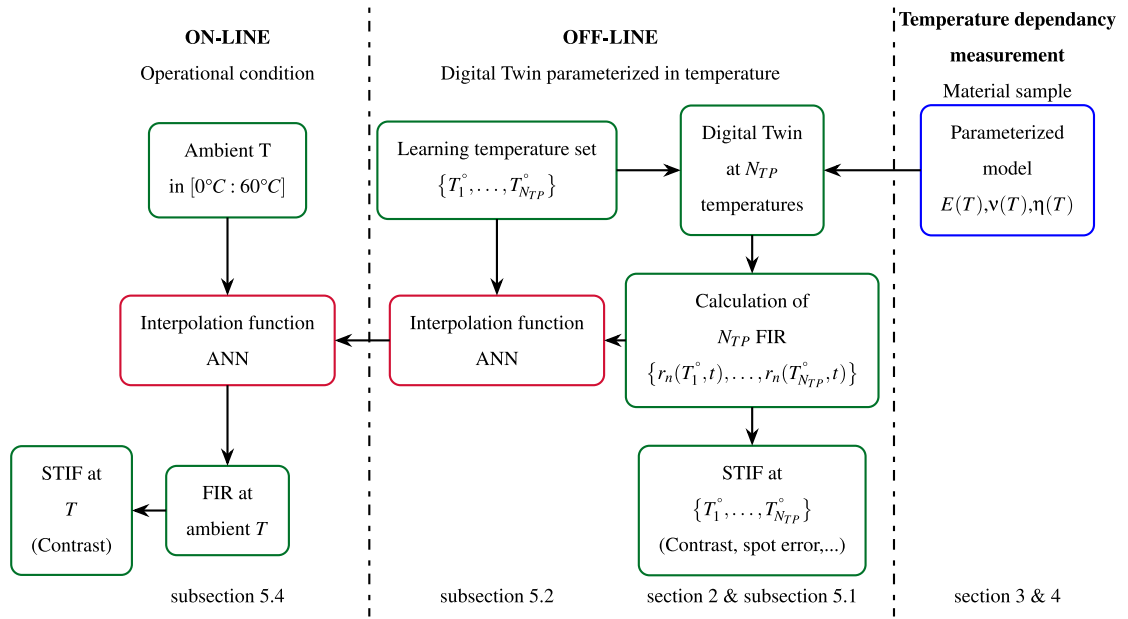
Fig. 1. Schematic of the overall process for understanding and compensating temperature effects on the STIF method. The right column represents the determination of the parameters dependency with the temperature. The center column illustrates the "off-line" process, allowing to calculate a set of N_{TP} FIR filters thanks to the digital twin parameterized in temperature, and the training of an interpolation function (AN). Finally, the left column represents the "on-line" process, with the ANN allowing to compensate for the temperature in real time.

In [27,28], the authors compared several models such as auto-regressive (ARX) dynamic model, static linear, bi-linear, quadratic, third and fourth order polynomials, and the latter gives the best reproduction capabilities. Other studies use machine learning, such as Support Vector Machines (SVM) in [29] and Artificial Neural NetWorks (ANN) in [30–32]. More recent studies as [33] propose a comparison between MLR, SVM and ANN for non uniform temperatures distribution in the cross-section of structures and show that in this case the SVM is the fastest regression method. Moreover, Jang et al. [34], compared MLR, Random Forest, ANN and SVM, on a numerical model of bridge heated by temperature models such as the one presented in [35]. Finally a bayesian framework able to link the modal properties with the damage parameter and temperature is proposed in [36]. Temperature compensation approaches in those neighboring areas thus largely rely on machine learning algorithms to discover the nonlinear relationship between temperature and functions to be compensated. For the case of bending wave focusing algorithms, no studies related with the effects of temperature and associated mitigation procedures allowing to compensate for it have however been reported in the literature to the knowledge of the authors.

Therefore, we propose here to study the effects of temperature on a bending wave localization method (the STIF method [11,12]) applied to materials representative of the automotive industry (polypropylene) and to develop an associated mitigation procedure based on machine learning to compensate for them. In the specific context of audio reproduction for automotive applications, the requirements associated with the STIF method and the associated temperature compensation method are the following one:

- The bending wave focusing should be precise in terms of spatial focusing and signal phase reproduction regardless of temperature,
- The proposed compensation method must be robust and inexpensive in terms of computational resources because embedded in a car calculator,
- The learning phase must be achieved with the minimum of input data, because of the difficulties to perform several in situ experiments allowing to learn the dynamics for various temperatures.

Consequently, the scientific objectives of the present study are (see Fig. 1):

1. To set up a process based on mode tracking and identification that will allow for the characterization of the temperature effects on the dynamics of a vibrating polypropylene plate representative of automotive applications, and to extract the temperature dependency of its material parameters, namely the Young's modulus, the loss factor, the Poisson's ratio and the mass density,
2. to use these temperature dependency laws to quantify the influence of the temperature on the bending wave focusing method (STIF method) by using a digital twin driven by these temperature dependency laws,
3. and finally to compensate for those effects by setting up an artificial neural network controller trained on the digital twin parameterized in temperature and able to predict the adequate STIF filters for any arbitrary working temperature.

The paper is organized as follows. Firstly, in Section 2, the spatio-temporal inverse filtering (STIF) method will be presented and applied on a numerical example (called here the *digital twin*) for demonstration purposes and called digital twin. Secondly, in
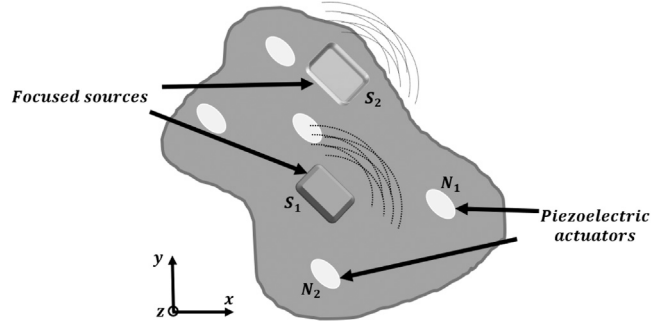
Fig. 2. Arbitrary shaped-like structure with piezoelectric actuators and localized audio sources.

Section 3, a procedure based on experimental mode tracking is set up to study the influence of the temperature on the dynamic of a polypropylene plate sample. Thirdly, in Section 4, a model updating strategy is adopted to extract the temperature dependency law of the material properties. The objective is to precisely know how the material parameters of the polypropylene vary with temperature to be able to build a physically realistic digital twin. Finally, in Section 5, a temperature compensation strategy based on an artificial neural network trained by the digital twin parameterized in temperature is used to compensate for the effects of temperature.

2. Bending wave focalization

As stated in Section 1, several methods able to invert the spatiotemporal propagation operator exist in the literature. The methods differ depending on the available knowledge of wave propagation in the plate they rely on. The Modal Control (MC) approach relies on a theoretical knowledge, the second method, referred as Time Reversal (TR) relies on partial spatial knowledge, and the last one named Spatio-Temporal Inverse Filter (STIF) is based on a full spatial knowledge of the propagation operator. In this section, only the STIF will be presented and studied here, because it presents superior performances in the current context, as already demonstrated in [17].

2.1. Problem statement

Let S denote a plate-like structure of arbitrary shape and with arbitrary boundary conditions. Assuming that this structure lies in the (x, y) plane, the positions of the N actuators (piezoelectric or audio exciter) bonded on S are given by $\{(x_n, y_n)\}_{n \in [1,N]}$ and the out-of-plane displacement of the plate at the temperature T is denoted as $u(x, y, t, T)$ (see Fig. 2).

The objective is now, for any input audio signal $a(t)$ and actual temperature T, to focus the bending wave field $u(x, y, t, T)$ to fit a given target shape $\phi(x, y)$ using the N actuators through N FIR filters $r_n(t, T)$ applied to the audio input. Mathematically, this means that we would like to achieve:

$$\forall t, T \; u(x, y, t, T) = \phi(x, y)a(t). \tag{1}$$

Or equivalently in the frequency domain, with $U(x, y, f, T)$ and $A(f)$ the Fourier transforms of the displacement and the audio signal respectively:

$$\forall f, T \; U(x, y, f, T) = \phi(x, y)A(f). \tag{2}$$

Assuming the system is globally linear (the path between an actuator and a sensor is considered as linear), the contributions $u_n(x, y, t, T)$ of all the N actuators generating the field $u(x, y, t, T)$ sum up and can be written as:

$$\forall t, T \; u(x, y, t, T) = \sum_{n=1}^{N} u_n(x, y, t, T) = \sum_{n=1}^{N} h_n(x, y, t, T) * r_n(t, T) * a(t), \tag{3}$$

where "$*$" stands for the convolution product and $h_n(x, y, t, T)$ is the spatio-temporal impulse response of the nth actuator. Or equivalently in the frequency domain:

$$\forall f \; U(x, y, f, T) = \sum_{n=1}^{N} U_n(x, y, f, T) = \sum_{n=1}^{N} H_n(x, y, f, T)R_n(f, T)A(f). \tag{4}$$

By combining both expressions (2) and (4) of $U(x, y, f, T)$, the objective to achieve is then expressed in the frequency domain independently of the input signal $a(t)$ as:

$$\boxed{\text{Find } \{R_n(f, T)\}_{n \in [1,N]} \text{ such that } \forall f, T, \phi(x, y) = \sum_{n=1}^{N} H_n(x, y, f, T)R_n(f, T).} \tag{5}$$
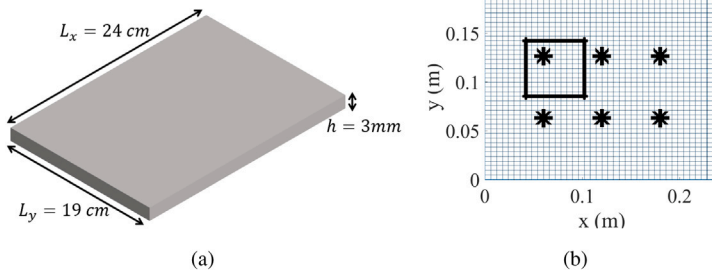
Fig. 3. (a) Dimensions of the plate and (b) meshes of the studied plate.

This means that the spatio-temporal propagation operators $H_n(x, y, f, T)$ associated with the N actuators and at a given temperature T needs to be inverted to design the N FIR filters $R_n(f, T)$ able to focus the bending wave field on the target shape $\phi(x, y)$ whatever the frequencies f contained within the input audio signal $a(t)$. In practice, focusing the bending waves thus consists in finding for each frequency and temperature the adequate phases and amplitudes to drive coherently each actuator bonded on the structure at the temperature T.

2.2. Spatio-temporal inverse filtering formalism

In this section, an effective method able to invert the spatiotemporal propagation operator $H_n(x, y, f, T)$ is presented. This method is based on a full spatial knowledge of the operator and is named Spatio-Temporal Inverse Filter (STIF). Let assume that a complete spatial knowledge of the propagation operator is available for temperature T. More precisely, it is assumed here that the spatio-temporal operator is known for any actuator $n \in [1, N]$ and that measurements are performed over a complete grid of K points on the structure for positions $\{(x_k, y_k)\}_{k \in [1, K]}$ at a given temperature T. Mathematically, what is known in the frequency domain is $\{H_n(x_k, y_k, f, T)\}_{n \in [1:N], k \in [1, K]}$.

The problem to be solved can then be rewritten on the measurement spatial grid as:

$$\phi(x_k, y_k) = \sum_{n=1}^{N} H_n(x_k, y_k, f, T) R_n(f, T). \tag{6}$$

Thus, in the matrix form:

$$\boldsymbol{\Phi} = \mathbf{H}(f, T)\mathbf{R}(f, T). \tag{7}$$

The resulting matrix can first be directly pseudo-inversed in the frequency range of interest by keeping only large enough eigenvalues. This leads directly to the FIR filters $R_n(f, T)$:

$$\mathbf{R}(f, T) = \mathbf{H}(f, T)^+ \boldsymbol{\Phi}, \tag{8}$$

where "+" denotes the pseudo-inversion operator.

It is important to note that the pseudo-inversion step is sensitive to noise. Hence, during the pseudo-inversion step, the lowest singular values are canceled to deal with those matrix conditioning issues. More details are available in [37].

This method offers several advantages. Firstly, the method is robust because it allows acquiring information about the wave propagation in the whole media. Moreover, the filters are computed by working on raw transfers directly instead of modeling the structure analytically or doing modal identification procedures. This allows to choose the filter size by sub-sampling in the frequency domain the transfers. Finally, this method is very interesting for its ease of implementation. Nevertheless, the points evoked above are also sources of drawbacks. Indeed, it is necessary to realize several experiments between all the points of the structure and the actuators and for several working temperatures, this complicates numerically the method. Moreover, the method is sensitive to the noise, mainly during the pseudo-inversion step. Thus, it could need a regularization step which is numerically heavy.

2.3. Illustrative numerical application

2.3.1. Structure under study

This subsection allows to illustrate the STIF method on a test case studied in a precedent article [17] for illustration purpose. The material used is polypropylene, with a Young modulus of $E = 1.1$ GPa, a Poisson's ratio of $\nu = 0.33$ and a density of $\rho = 990$ kg/m^3 (Fig. 3a). The studied plate is relatively damped with a damping ratio of 3%, and therefore different from the most frequently handled cases in the literature related with spatiotemporal inverse filtering which involve very low damped structures such as metal plates [9] or smartphone glasses [38].

The plate is modeled with shell elements and presented in Fig. 3b with the position of the actuators. The number of actuators and their positions are chosen to excite the 6 first modes in the frequency band of interest which is [100 Hz; 500 Hz]. The target
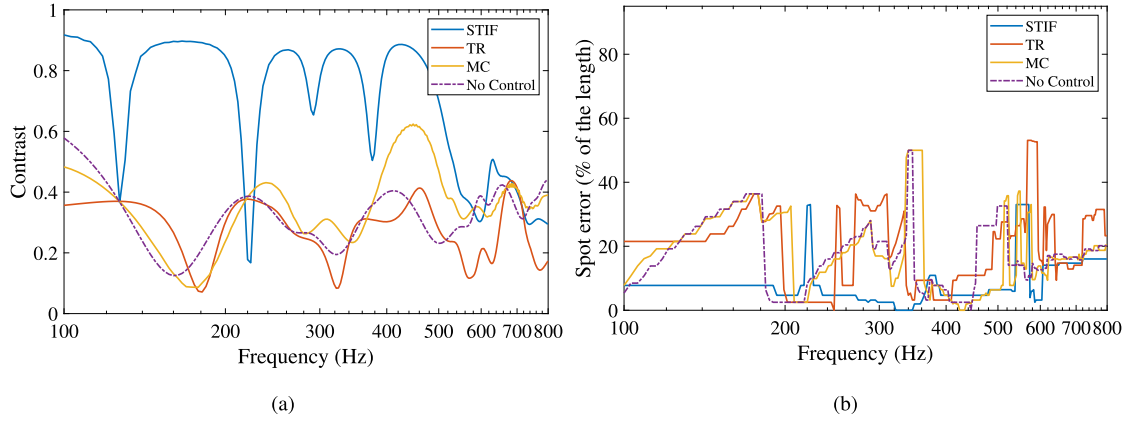
Fig. 4. (a) Contrast and (b) spot error for the simple plate.

shape is also shown in Fig. 3b, and consists in a rectangle of size $(0.25L_x, 0.3L_y)$ and centered at $(0.3L_x, 0.55L_y)$. The targeted displacement is 1 inside the target shape and 0 outside. The audio signal to be reconstructed is a sweep sine with a duration of 2 s, spanning frequencies from 100 Hz to 800 Hz, sampled at 44.1 kHz. The chosen frequency range allows to excite the 6 first modes. Modal properties of the structures are computed thanks to a finite element model implemented on the software SDT (SDTools©, Structural Dynamics Toolbox [39]). The STIF algorithm is developed and implemented in Matlab with SDT software jointly.

This model will be called the digital twin at a working temperature throughout this paper. It will be used as a virtual mean to experiment the effect of temperature on the STIF method and will thus allow to provide all the necessary data for transfers and FIR estimations. It will replace real work measurements for the purpose of this manuscript.

2.3.2. Key performance indicators

Two key performance indicators (KPI) will be used in order to assess the STIF method performances at various temperatures T comprised between 0 °C and 60 °C. Keep in mind that $u(x, y, t, T)$ is the out-of-plane displacement of the plate and $U(x, y, f, T)$ its Fourier transform.

Spot error: given a reconstructed target shape, the first criterion is the measurement between the center of the target shape and the maximum amplitude of the reconstructed shape. Thus, the lower the distance, the greater the spatial localization accuracy.

Spatial contrast: the second criterion is the computation of the contrast between the energy in the reconstructed area (S_R) and energy of the total area ($S_T = L_x \times L_y$), so that:

$$C(f, T) = \frac{\int_{S_R} |U(x, y, f, T)|^2 \mathrm{d}S}{\int_{S_T} |U(x, y, f, T)|^2 \mathrm{d}S}. \tag{9}$$

If $C(f, T) = 1$, then all the energy is present in the target shape and nothing outside, and if $C(f, T) = 0$, then all the energy is outside the target shape.

2.3.3. Results

In this subsection, an example is detailed in order to illustrate the performances of the STIF algorithm. To that end, the results provided by the STIF algorithm are compared to the ones provided by the MC and TR algorithms and a no control case, where only the nearest actuator to the target shape is actuated, to be used as a reference. The MC consists in deriving analytically the FIR filters, while the TR is based on the time reversal concept. For more details regarding MC and TR methods implementation, the reader is referred to [17]. The spot error and the contrast in the frequency band [100 Hz; 800 Hz] for each method are plotted in Fig. 4. We can observe that the STIF method allows achieving a very high localization performance, in comparison with others. Indeed, it shows a contrast around 0.9 until 540 Hz. Moreover, it shows a very low spot error, which is around 12 % of the total length in the [100 Hz; 220 Hz] region, and lower than 10 % above 220 Hz approximately until 540 Hz. This can be explained by the fact that there are 6 modes until 540 Hz, so that 6 actuators are not sufficient to address and control more modes in the frequency band [100 Hz; 800 Hz]. The dips in the contrast curve and the peaks in the spot error curve correspond to the modal frequencies of the host structure. More details are provided in [17], and this section is to introduce the reader with the STIF method.

Now that the STIF method has been introduced, a methodology to study the effect of the temperature on a material representative of automotive applications will be presented in Sections 3 & 4, and the compensation for those effects on the STIF algorithm previously described will be presented in Section 5.
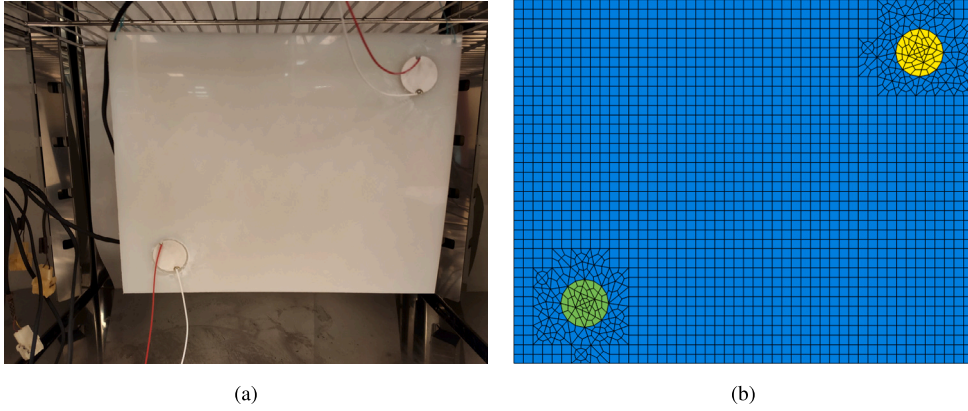
Fig. 5. (a) Physical plate in the oven and equipped with two piezoelectric elements and (b) its associated digital twin (multiphysical FE model).
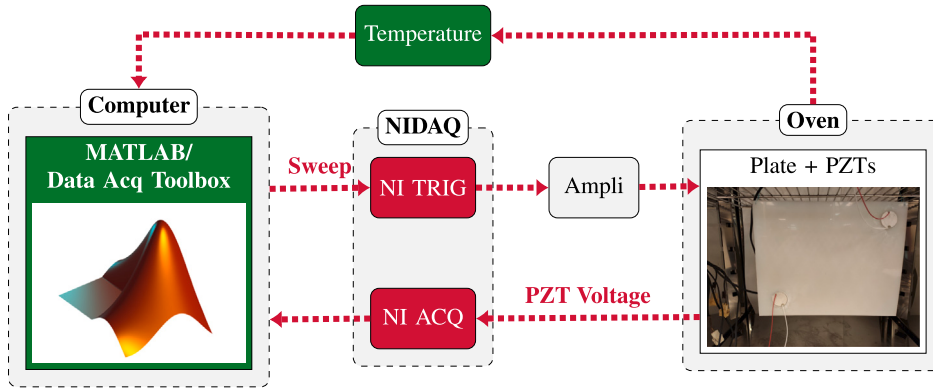

Fig. 6. Schematic summarizing the experimental protocol.

3. Experimental study of the influence of temperature on a polypropylene plate representative of automotive applications

3.1. Experimental setup and associated FE model

A rectangular polypropylene plate of size 24 cm × 19 cm × 3 mm representative of automotive applications will be used to study the effect of temperature on the material properties of polypropylene. This plate is assumed to be homogeneous and isotropic. The experimental setup consists in a plate equipped with two piezoelectric actuators Noliac NCE51 [40] glued with a cyanoacrylate adhesive and put in an oven, as shown in Fig. 5a. Moreover, an associated multi-physics finite element model is presented in Fig. 5b for validation purpose. The plate and the PZTs are modeled by shell elements with Matlab and SDT (SDTools©, Structural Dynamics Toolbox [39]). The main idea here is to extract the temperature dependency laws of the material parameters of polypropylene through the variations of the modal properties of the plate.

As shown in Fig. 5a, the plate under study is put in a temperature regulated oven, allowing to apply controlled temperature variation on the plate. It is important to note that the plate is thin and assumed isotropic and homogeneous so that there is no temperature gradient during the heating process. The plate is subjected to a temperature cycle during 3 h, varying from 0 °C to 60 °C, with a slope of 0.4°/min during which the temperature inside the oven is acquired in real time. This temperature program is assumed to be slow enough to consider that the plate temperature is the same as the oven temperature. Moreover, the plate is equipped with two piezoelectric elements (PZT), the upper right one allowing to excite it dynamically and the lower left to acquire the deformation corresponding to the waves propagating within the plate. The piezoelectric elements were disposed this way to maximize the modal observability and controlability [41]. Finally, the plate is suspended on the grid of the oven by nylon strings. This type of string is damped and allows to come as close as possible to the "free–free" boundary conditions by reducing the coupling with the oven.

The experiment consists in sending a sine sweep of frequency varying from 100 Hz to 1500 Hz, sampled at 8500 Hz, through the upper right PZT, and acquiring the plate response using the second PZT. The acquisition hardware is composed of a NI-cDAQ-9178 rack, enabling to trig the signal, and a NI-9234 acquisition card mounted on it to acquire the input and output signals each 2 °C. The schematic summarizing the experimental protocol is provided in Fig. 6.

It is important to notice that according to the used NCE51 PZT actuator datasheet,[1] the Curie temperature of the PZT elements is 360 °C. Moreover, relative variations of the permittivity and coupling factors are lower than 10% in the studied temperature range 0 °C–60 °C. Finally, as the quantities measured and representing the dynamical behavior of the plate are its modal frequencies and damping, they are not sensitive to the effect of temperature on PZT, which is small as stated before. In conclusion, the major effect of temperature here is to induce variation of the mechanical properties of the polypropylene.

3.2. Results

The experimental results, corresponding to the voltage output of the PZT as a function of time and temperature, are given in Fig. 7a. Moreover, the Fig. 7b shows the amplitude and the phase of the frequency response functions (FRF), computed thanks to the estimator $\hat{H}_1(f) = \hat{G}_{yu}(f)\hat{G}_{uu}(f)^{-1}$. Where $\hat{G}_{yu}(f)$ represents the interspectrum of the input u and the output y, $\hat{G}_{uu}(f)$ represents the autospectrum of the input u [42].

In the working frequency band [100 Hz; 1500 Hz], one can notice a significant eigenfrequency shift. Indeed, there is a high decrease of the frequencies when the temperature increases. For example, the mode at around 900 Hz at 10.1 °C decreases to approximately 700 Hz at 40 °C. Furthermore, the amplitude peak decreases until 22.5 °C, and increases from this temperature, forming a kind of "U curve". Moreover, the mode width is getting larger and then thinner again. All these results show a significant effect of temperature on the dynamics of the plate which are related to an evolution of its material properties: the higher the temperature, the softer the material becomes.

4. Construction of an updated FE model taking into account the temperature effects

4.1. Procedure overview

The schematic summarizing the approach being adopted in the following of this study to build an updated FE model representing the dynamical behavior of the polypropylene plate with the temperature is shown in Fig. 8. This part will also present the post-processing of the previously acquired experimental data. The first step is the extraction of the modal parameters of the structure, such as the experimental modal frequencies $f_p(T)$ and the damping ratios $\zeta_p(T)$, by fitting the frequency response functions (FRFs) thanks to a modal identification procedure referred to in the literature as Experimental Modal Analysis (EMA). During the second step, a multiphysical FE model is built containing the plate modeled as shell elements and the PZTs glued on it (see Section 3.1). This model will allow for the computation of the transfer functions between the PZTs for several sets of parameters $(E(T), \nu(T), \zeta(T))$. Finally, an objective function is defined, based on the minimization of the relative error between the experimental identified and the numerical updated FRFs. The main objective is thus to get the temperature dependency of the polypropylene material properties.

4.2. Extraction of the modal parameters

Several estimation methods for modal identification are available in the literature. The idea is to find a model fitting the experimental data to get the associated modal parameters. The identification method used here is based on local peak-picking mode identification and large band estimation using the pole/residue model. After identifying a set of poles, an non-linear optimization of poles and residues is done in the frequency band of interest according to [43]. More details regarding this methods and the related procedures are provided in [43–45].

Starting from the classical second order mechanical state space model with real coefficients, it can be shown [43] that the relation between inputs and outputs can be expressed in the form :

$$[H_{id}(s)] = \sum_{j \in identified} \left(\frac{[R_j]}{s - \lambda_j} + \frac{[\overline{R}_j]}{s - \overline{\lambda}_j} \right) + \frac{[F]}{s^2} + [E],$$ (10)

this parameterization is called the pole/residue model with $s = i\omega$, ω being the circular frequency and λ_j is the jth pole. The residue is written as $[R_j] = \{c\phi_j\}\{\phi_j^T b\}$, namely the product of a column vector $\{c\phi_j\}$ (modal observability at sensors) and a row vector $\{\phi_j^T b\}$ (modal controlability at loads). Note that in the literature, $\{c\phi_j\}$ is also referred to as mode shape $\{\phi_j\}$ and $\{\phi_j^T b\}$ as participation factor $\{L_j\}$.

Because identification only focuses on specific frequency bands, the sum (10) is truncated. The term $E(s)$ called flexibility takes into account the contribution of higher frequency modes (constant asymptotic term for displacement/force) and $F(s)$ called inertia takes into account the contribution of lower frequency modes such as rigid body modes ($1/s^2$ asymptotic term).

As stated previously, an initialization step is firstly performed. Indeed, a local peak-picking identification is done for each resonances separately using the pole/residue model, followed by a large band estimation, and so forth. This is done until having a number of modes consistent with the FE model. From this initialization of the set of poles, the next step is to perform a non-linear
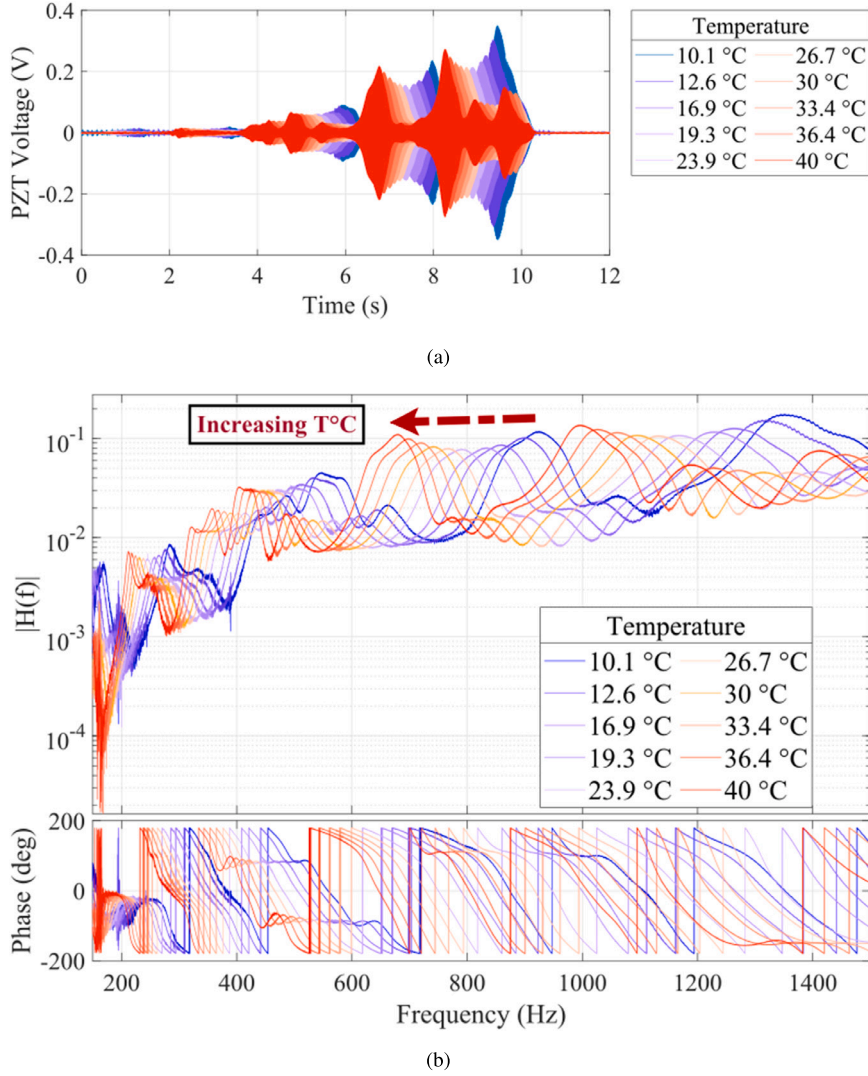
---

[1] Datasheet link here.

Fig. 7. (a) Evolution of the response of the lower left PZT in the time domain and (b) frequency response function between the two PZT, for several temperatures.

optimization of the λ_j parameters to reach the minimum of the cost function leading to an optimized set of poles and associated residues:

$$J(R_j(\lambda_j), E, F) = \left| [H(s)]_{test} - \sum_{j=1}^{NM} \left(\frac{[R_j]}{s - \lambda_j} + \frac{[\overline{R}_j]}{s - \overline{\lambda}_j} \right) + \frac{[F]}{s^2} + [E] \right|^2 ,$$

(11)

where $[H(s)]_{test}$ is the experimental FRF compared to the "pole/residue" model. The whole procedure is achieved thanks to the Matlab toolbox SDT (SDTools©, Structural Dynamics Toolbox [39]).

The Fig. 9, presents an example of an identification using the SDT modal identification: in blue the experimental FRF is shown and in red the synthesized transfer from identified poles and residues. This procedure is performed for each temperature, and the identified poles are stored. It can be seen that the peaks are very broad leading to modal coupling between closed modes and making the identification quite tricky for polypropylene material.

The eight modal frequencies extracted span the band [307 Hz, 715 Hz] at 0 °C and [182 Hz, 416 Hz] at 60 °C. Furthermore, the identification results are plotted in Fig. 10 which shows the absolute damping $\zeta(T)$ and relative frequency evolution $(f(T_i) - f(T_{ref}))/f_{ref}$ with the temperature ($T_{ref} = 25.4$ °C). It can be seen that the frequency is highly decreasing with the temperature, with a similar evolution for the eight modes. The relative frequency is about 30% higher at 0 °C and approximately 20% lower at 60 °C than the value taken at the reference temperature $T_{ref} = 25.4$ °C. We note moreover that the evolution of the modes is very similar, which is expected since the material can be considered as isotropic and that we therefore have a dependence on the evolution of the Young's modulus $E(T)$ which impacts all modes in an equivalent way. The small deviations can be explained by a
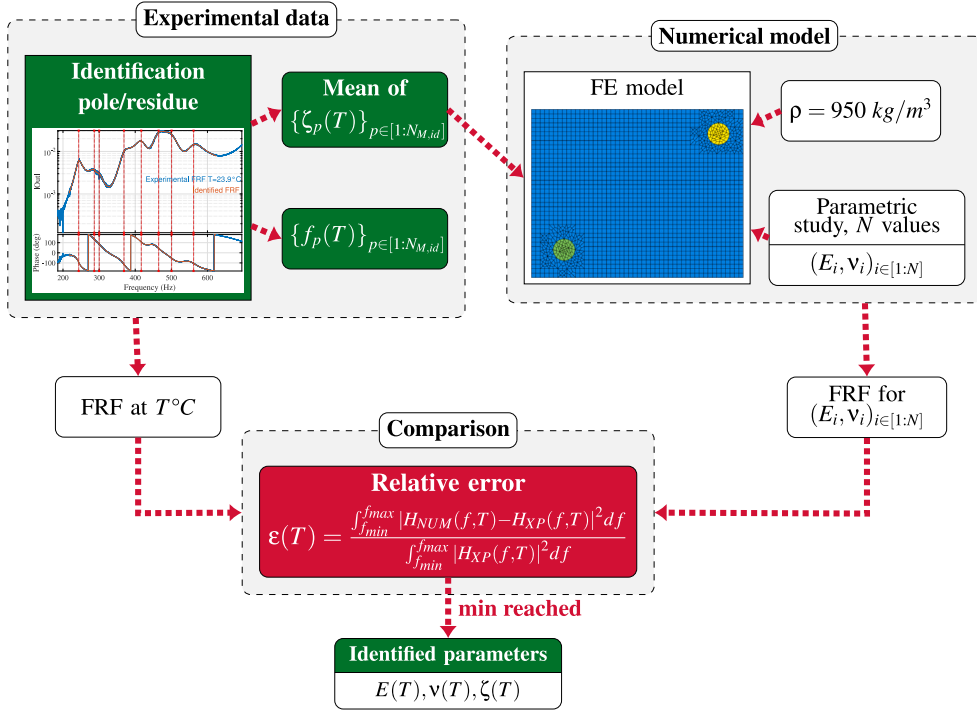
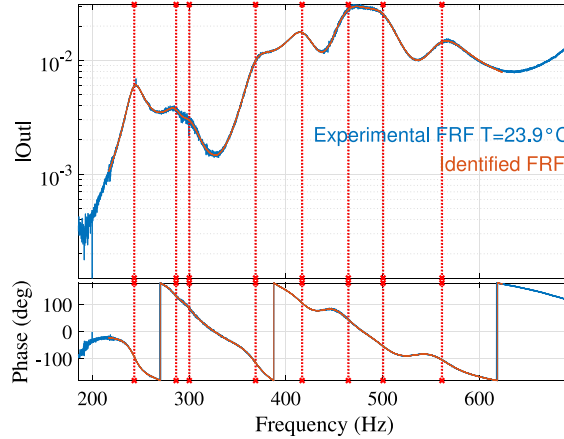Fig. 8. Schematic summarizing the approach for model updating of the plate.

Fig. 9. Example of modal identification.

possible degree of anisotropy, a temperature gradient in the plate or an identification bias. Moreover, the damping ratios increase from 2%–2.5% until 3.5%—5% at around 20 °C, and then decrease under 2%. Hence, there is a relation between the damping and frequency evolution, so that the damping ratio maximum coincides with the sharpest slope point of the frequency curve. This behavior is characteristic of the material transition from a glass state to a rubber state, and the middle temperature of this transition zone is around $T_g = 20$ °C. These observations are classical in the analysis of material parameters evolution with temperature, see the Refs. [20,46].

These results will be used in the following subsection to create an updated numerical model taking into account these temperature effects.

4.3. Model updating procedure

After building a FE model, it is crucial to ensure its fidelity with respect to experimental data. To that end, the test-analysis correlation allows to update the model parameters. More details about dynamical model updating procedures are available in [47].
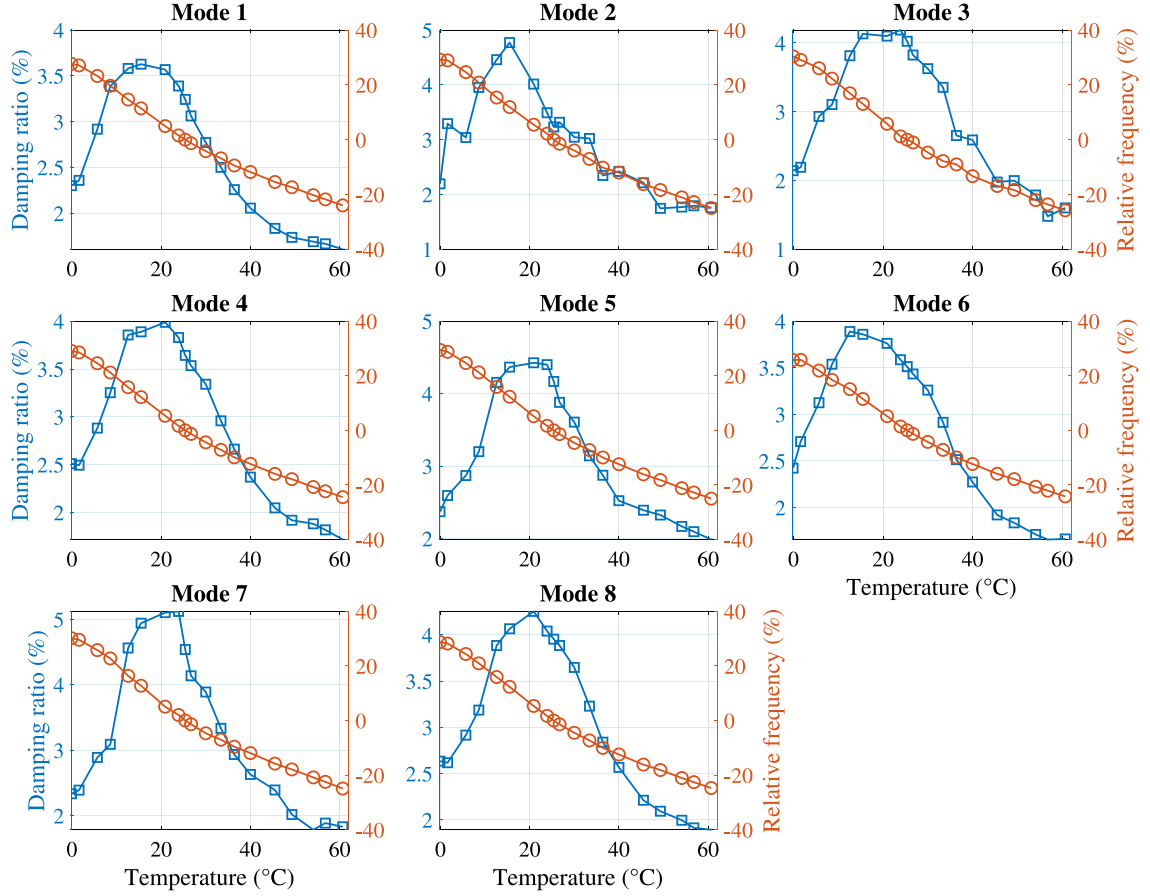
Fig. 10. Evolution of damping ratios and natural frequencies for the first eight modes as a function of the temperature, from the modal identification.

There are several objective functions to be used for comparing experimental and numerical data: (i) the quadratic norm on frequency errors, and/or the shape correlation error with the MAC (Modal Assurance Criterion [48]) ; (ii) the energy error ; (iii) the comparison between the experimental and numerical FRFs. This last approach will be used here. It has several benefits, such as the ability to process highly damped models and high modal density (by working directly on the measured raw data).

The retained assumptions for this study are a simple plate with an homogeneous and isotropic material. Consequently, there are four material parameters to tune: the density ρ, the complex Young's modulus $E(1 + j\eta)$, and the Poisson's ratio ν. Firstly, knowing the dimension of the plate (24 cm × 19 cm × 3 mm) and the mass after weighing it (130 g), the material density is deduced as $\rho = 950$ kg/m³. Secondly, only the real part E of the complex young modulus is to be updated. Indeed, in the case of isotropic and homogeneous materials, there is a direct relationship between the modal damping ζ and the loss factor $\eta = 2\zeta$. The viscous damping ζ is chosen as the mean of the damping corresponding to the eight first identified modes.

Thus, the two remaining parameters E and ν will be chosen such that the following error will be minimized:

$$\{E(T), \nu(T)\} = \arg\min \frac{\int_{f_{min}}^{f_{max}} |H_{NUM}(f, T, E(T), \nu(T)) - H_{XP}(f, T)|^2 df}{\int_{f_{min}}^{f_{max}} |H_{XP}(f, T)|^2 df}, \tag{12}$$

with $H_{NUM}(f, T, E(T), \nu(T))$ the numerical FRF depending on temperature, frequency, Young modulus and Poisson's ratio. $H_{XP}(f, T)$ denotes the experimental FRF and depends on the temperature and frequency. It is not common to update the Poisson's ratio in the literature, but on this test case, it has a very high impact on modes. It will be analyzed in the following sections.

4.4. Model updating results

The model updating results for two temperatures are given in Fig. 11 for $T = 5.7$ °C and $T = 33.4$ °C, and are superposed with the corresponding experimental FRF. Model updated results are very similar to the experimental ones, both in terms of amplitude and phase. It shows also that the polypropylene material composing the plate is very damped, causing very broad peaks and modes almost combined together.
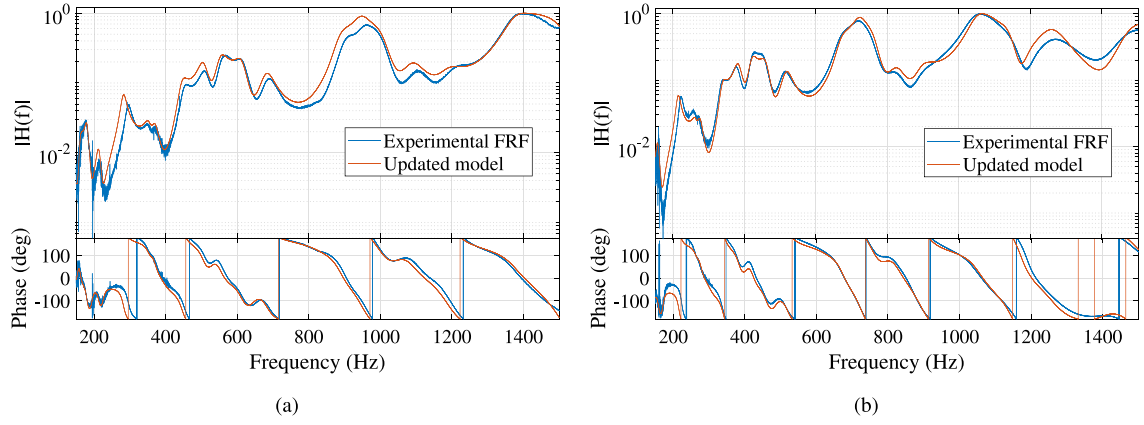
Fig. 11. Superposition of experimental and numerical updated model for (a) $T = 5.7$ °C and (b) $T = 33.4$ °C.
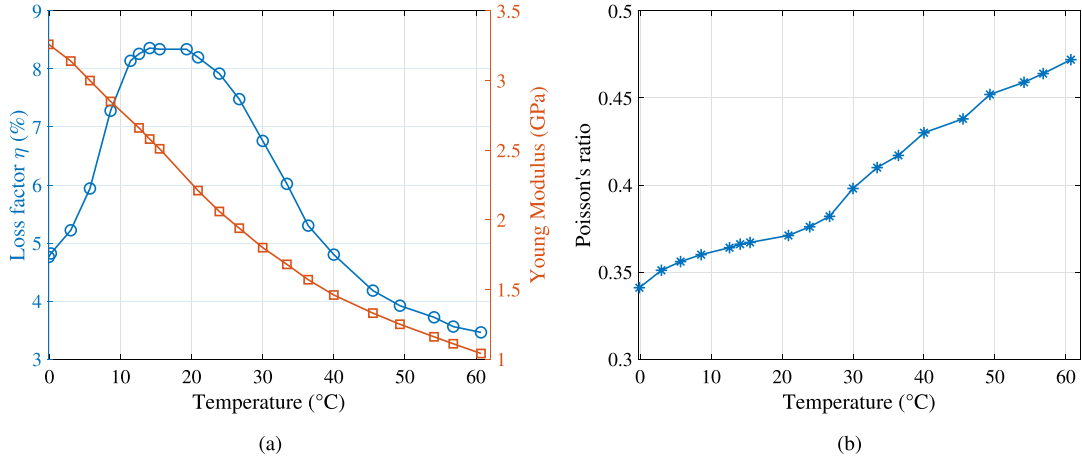

Fig. 12. Results of the model updating, for (a) damping ratio and Young Modulus, and (b) for Poisson's ratio according to the temperature.

The loss factor η and the Young's modulus E are presented in Fig. 12a and the Poisson's ratio in Fig. 12b. It can be seen that the Young's modulus varies strongly with temperature. Indeed, the polypropylene becomes softer with temperature, leading to a decrease in stiffness from 3.25 Gpa at 0 °C to 1 Gpa at 60 °C. The loss factor is maximal in the interval [10 °C, 20 °C] with a value of 8.5%. It decreases outside, with a value of 4.8% at 0 °C and about 3.5% at 60 °C. These values are very high due to the material, which makes identification and updating more difficult as previously mentioned. Moreover, the Young's modulus pattern follows the modal frequencies evolution. As discussed in Section 4.2, this behavior is typical to glass transition in this temperature range.

As previously stated, it is not common in the literature to update the Poisson's ratio. As a reminder, this coefficient represents the deformation of a material in a perpendicular direction to the loading direction. However, in order to get a good agreement between the experimental and numerical FRFs, the tuning of this parameter was crucial in this study. It was found here that it increases from the common value 0.34 to approximately 0.475, showing that the material is in a phase transition and is tending to its rubber state (as stated in Section 4.2). Hence, the variations of this parameter are very important and should be taken into account. It is worth mentioning the study [20], where the variation of the Poisson's ratio with temperature of poly(butylene terephthalate) is studied in an experimental way thanks to a biaxial contact extensometer. The presented results are consistent with the ones obtained here in terms of Young modulus and Poisson's ratio range variation and order of magnitude.

Finally, the excellent agreement between the experimental data and the numerical model will allow to predict with a good precision the effect of the temperature on the bending wave focalization algorithm. This is the subject of the following section.

5. Temperature influence on the STIF method and associated compensation procedure

As explained previously in Section 2, the STIF method requires a learning phase where the dynamics of the structure must be learned for several temperatures. Thus, if we take as an example a car door panel, for a given number of temperatures N_{TP} ranging from 0 °C to 60 °C, we will have to perform and process $N_{TP} \times N_{sensors} \times N_{actuators}$ laser vibrometer measurements. To overcome

Table 1

Material properties for the PP plate at 20 °C.

Temperature	E (GPa)	ν	η (%)	ρ (kg/m³)
20 °C	2.26	0.37	8.2	950
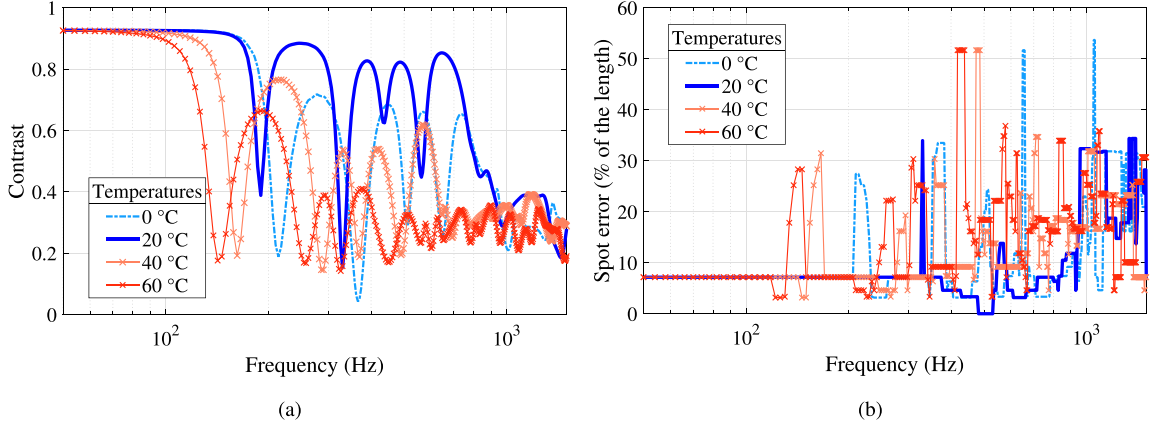
Fig. 13. (a) Contrast and (b) spot error without temperature compensation of the STIF method.

these limitations, the main idea here is to replace the N_T experiments by a smaller number, and to find a non-linear function to determine a filter associated with any temperature in the interval [0 °C, 60 °C]. In our case, the real conditions are replaced by numerical experiments using the updated digital twin defined at Section 2, and parameterized by the temperature dependency laws of the material properties determined in Section 4.

5.1. Bending wave focusing before temperature compensation

To begin with, it is important to evaluate the performances of the STIF algorithm without taking into account the influence of temperature. The digital twin described in Section 2 and parameterized in temperature with the dependence laws of the polypropylene will be used to achieve this goal.

To do so, a unique FIR filter is built at a temperature of 20 °C (for the 6 actuators), using the parameters previously identified, available at Table 1.

Then, the bending wave focalization procedure is performed using the FIR coefficients at 20 °C on the digital twin for several temperatures from 0 °C to 60 °C each 5 °C. The results and performances of the algorithm are shown in Fig. 13 using the two key performance indexes defined in Section 2, namely the contrast and the spot error, for 0 °C, 20 °C, 40 °C, and 60 °C.

It can be seen that the STIF method provides only satisfying focalization abilities for the learning temperature a T = 20 °C. Otherwise, the performances are highly degraded, mostly when the operating temperature is far from the learning one. For that reason, the next section will present a simple method based on an artificial neural network (ANN) to learn the nonlinear relations between the temperature and the FIR coefficients of the STIF method, in order to be able to adapt them to the actual temperature.

5.2. Presentation of the compensation strategy

This subsection discusses a compensation strategy to take into account the influence of temperature. FIR filters are computed for different temperatures, using the temperature-parameterized digital twin. From a practical point of view, it is possible to compute each FIR associated to a temperature every N_T°C between 0 °C and 60 °C, and then to train a neural network which will allow to determine the FIR filter for any temperature included in this interval. These filters can be obtained by experiments on a real structure, or in our case by a digital twin updated and parameterized in temperature. This neural network will be stored in the computer of the car for example. Thus, when the temperature sensor detects a temperature variation, the FIR set corresponding to this temperature is automatically determined by the neural network and loaded.

The chosen compensation strategy is therefore based on the use of artificial neural networks (ANNs). ANNs are well suited to our context because they allow us to design an output estimation function for a non-linear multiple input–output system, using nodes or (neurons) interconnected in a structure made of several layers. The input data is divided into three groups, namely training, validation and testing. The training group is used for learning, the validation for estimating generalization abilities. The test group then provides an overview of the performance without influencing the learning. The method is based on the optimization of coefficients called biases b and weights W that minimize a performance function based on the training dataset [49]. This performance function is defined as the error between the ANN outputs and the corresponding target outputs. In the case of a small amount of data and noisy datasets, and to avoid the problem of over learning, a method based on Bayesian regularization [50] will be used.
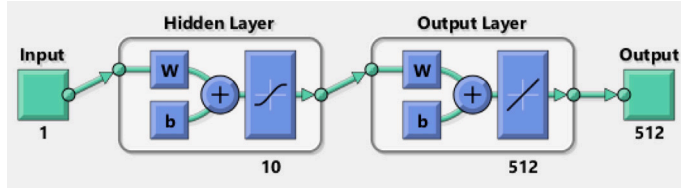
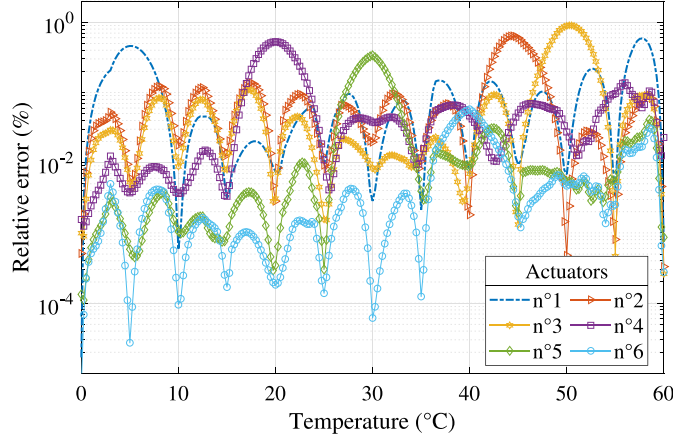**Fig. 14.** Neural Network schematic from Matlab.

Fig. 15. Prediction error regarding the FIR coefficients of the STIF method for several temperatures for the 6 ANNs corresponding to the 6 actuators.

The neural network is constituted by one input layer corresponding to the temperatures $\left\{ T_1^\circ, \ldots, T_{N_{TP}}^\circ \right\}$. In our case, the hidden layer is made by 10 nodes, and the influence of the number of retained nodes is analyzed thanks to a parametric study thereafter. Moreover, the output layer is composed by the 512 FIR coefficients corresponding to each input temperature. Those FIR are computed for a given actuator n by the digital twin parameterized in temperature, $\left\{ r_n(T_1^\circ, t), \ldots, r_n(T_{N_{TP}}^\circ, t) \right\}$. The temperature inputs and the corresponding FIR outputs are chosen every 5 °C. The activation function of the hidden layer is a tan-sigmoid function and the output layer one is a linear function. In this present study, the ANN is trained thanks to the Matlab's toolbox *"Artificial Neural Network"* with the Bayesian regularization training algorithm. The scheme of the ANN used is available Fig. 14.

Furthermore, the relative error between the real FIR and the reconstructed FIR for a temperature T and for an actuator n is given by :

$$ RE(T) = 100 \times \frac{\int_0^t (r_n^{NN}(t, T) - r_n^{real}(t, T))^2 dt}{\int_0^t (r_n^{real}(t, T))^2 dt}. \tag{13} $$

This will allow to quantify the performance and reproduction abilities of the trained ANN on a validation dataset.

5.3. Results for the trained ANN

In order to verify the generalization ability of the trained ANNs and to choose the best number of nodes, a set of FIR filters corresponding to temperatures ranging from 0 °C to 60 °C every 0.25 °C are computed via the digital twin.

First, as an illustration, the relative error Eq. (13) is plotted in Fig. 15 for each 0.25 °C for the FIR filters corresponding to the 6 actuators, and for an hidden layer of 10 nodes. First, the relative error is always lower than 0.9% for each temperature and for the 6 actuators, which is overall a very small error. Second, we can see that the error is minimal at the training temperatures, except for some temperatures used by the optimization algorithm for testing. As for example at 20 °C for actuator 4 or at 50 °C for actuator 3. We can conclude that the trained ANNs allow to reproduce very precisely all the FIR coefficients for a given input temperature.

Consequently, the evolution of the FIR coefficients with temperature in 3D is shown in Fig. 16 illustrating the nonlinear nature of the FIRs evolution with temperature and thus the difficulty in finding a function linking the inputs/outputs without machine learning.

5.4. Bending wave focusing performances after temperature compensation

The Fig. 17 shows the contrast and spot error after temperature compensation, by using the ANNs trained previously. It can be seen that for each temperature, the contrast and spot error are recovered and the performances are maximum and comparable to

(a) Actuator 1 (b) Actuator 2 (c) Actuator 3

(d) Actuator 4 (e) Actuator 5 (f) Actuator 6
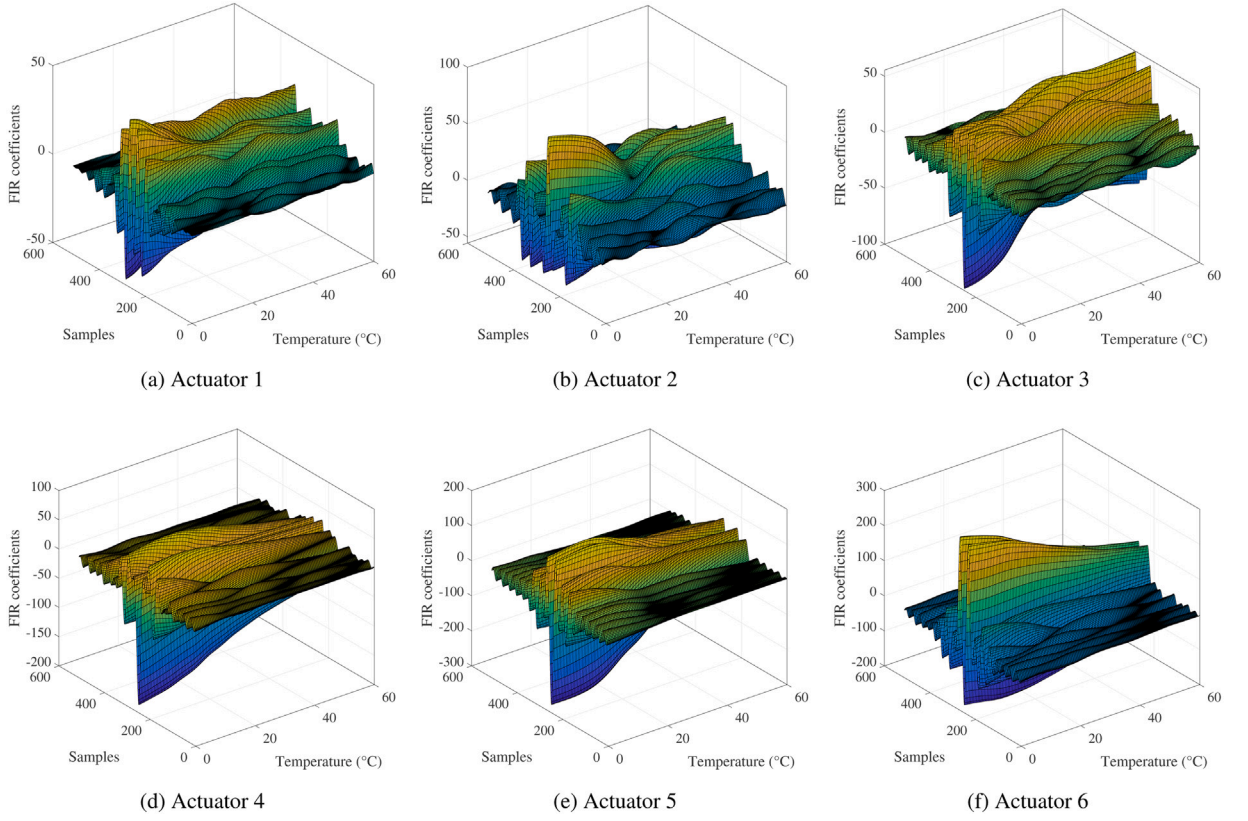
Fig. 16. Reconstructed FIR coefficients by the neural network according to the temperature, for the 6 actuators.

(a) (b)
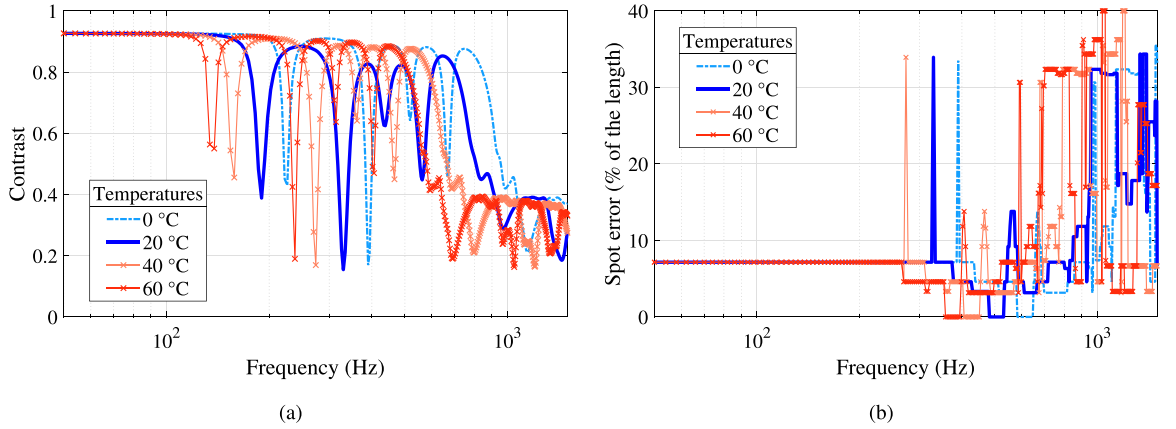
Fig. 17. (a) Contrast and (b) spot error after temperature compensation.

the ones shown in Section 2. Moreover, we notice that the restitution frequency band is variable. Indeed, the identification part showed that there is a shift of the eigenfrequencies with respect to the reference temperature (T_{ref} = 25.4 °C), which explains that due to the inherent properties of the material, there is a physical limitation to the contrast restitution.

5.5. Discussion about the choice of the parameters for the training phase

In the following, we present a parametric study to optimize the learning step, in terms of trade-off between the amount of input data and the desired performance.
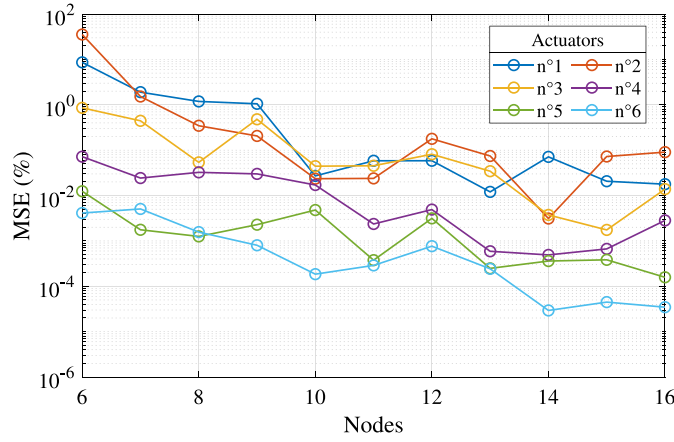
Fig. 18. MSE of the validation data trained with 6 to 16 hidden nodes.
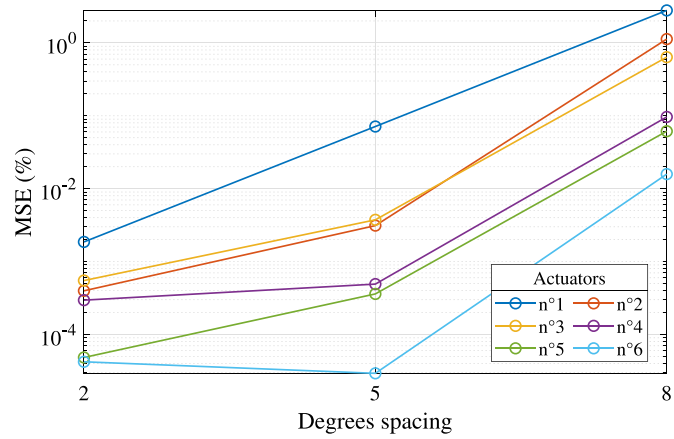

Fig. 19. MSE for a 14 nodes ANN and for three temperature spacing used for learning (2 °C, 5 °C, 8 °C).

To evaluate the overall generalization capability of ANNs as a function of the number of nodes, we compute the mean square of the relative error (RE) defined by the Eq. (13) on the validation temperatures (0 °C: 0.25 °C: 60 °C), for 6 to 16 nodes. The results are available in Fig. 18. It shows that for 9 nodes, the mean for each actuator is under 1%, and after 10 nodes it is less than 0.1%. This validates our choice of retaining ten nodes. Indeed, the computation time varies greatly, from 1 h for 10 nodes to 7–9 h for 16 nodes. During the training stage, the training data, validation and test are chosen randomly by the bayesian inference algorithm. Thus, depending on the initial choice, the error will converge more or less quickly and more or less accurately.

In addition, the number of learning temperatures is crucial to guarantee a good generalization capacity. The smaller the interval between learning temperatures, the better the generalization ability. Thus, three learning steps were performed for datasets with temperatures spaced every 2 °C, 5 °C, and 8 °C respectively, for each actuator and for 14 nodes. The Fig. 19 shows the mean square on the validation temperatures for these three different datasets. This spacing of 5 °C between each learning temperature is a good compromise between the cost of the experimental procedure, the cost of training the ANN and the accuracy of the ANN.

More than that, the number of FIR coefficients used to reproduce the target shape is also crucial. The number of 512 coefficients is chosen because it effectively reproduces the contrast and is low enough for real-time implementation. By taking less than 512 coefficients, the ANNs are trained faster but the contrast is poorly reproduced. On the other hand, the higher the number of coefficients, the more expensive the training will be in terms of computation and memory capacity. Indeed, it takes about 7–9 h for 16 nodes, with 512 coefficients, depending on the initial conditions (the computation time can be more or less high).[2] As these calculations are carried out in "off-line", there will be no consequences for the use in operational condition.

---

[2] The type of processor used : Intel(R) Xeon(R) Gold 6138 CPU.

In conclusion, the effects of temperature on a bending wave focusing method of a polypropylene plate have been studied, and a compensation procedure based on a digital twin have been validated. The first step is the realization of a qualitative study of the influence of temperature on a real test plate made of the target material. Thus, this plate was placed in an oven and uniformly subjected to different temperatures ranging from 0 °C to 60 °C. A modal identification based on the pole/residue parameterization allowed to extract the modal parameters as a function of the temperature. Then, a model update strategy is performed to extract the temperature dependency of the material parameters. The objective is to precisely know how the material parameters of the polypropylene vary with temperature to be able to build a physically realistic digital twin. This temperature dependency of the material is then injected into a digital twin plate which is modeled at Section 2 to simulate the measurements and so to study the focusing of the bending waves.

The digital twin studied in Section 2 and parameterized in temperature, is then used to study the influence of the temperature on the STIF algorithm. Indeed, the FIR filters computed for T = 20 °C on this numerical model and applied to other temperatures shows that the STIF algorithm works only for the temperature used during the training. Thus, ANNs were designed to establish a function between the temperatures and the associated FIR filters, allowing to load and use the appropriate filters for the current temperature of the car's trim. Indeed, the ANN training depends on the size of the FIR filters and the amount of training data. Thus, for 512 coefficients, the generalization ability is verified with training data spaced with an interval of 5 °C. This interval is a good compromise between accuracy, computational cost and the effort required for the experimental realization.

Nevertheless, some limitations must be underlined. First of all, the future work and perspectives is the test of the bending waves focusing with temperature compensation on a real experimental plate and then on a car door panel, in order to verify the radiated sound quality. For practical experimental reasons, this was not possible in this work. In particular, the ability to perform laser vibrometer tests while varying the temperature accurately. Moreover, the temperature variation is assumed homogeneous and static, thus it would be judicious to study the impact of a temperature gradient and the effect of a rapid evolution. Finally, it would also be necessary to take into account the other parameters that are difficult to control (coupling evolution, fatigue of the structural elements of the car, . . .), with piezoelectric elements allowing to monitor the health of the structure in question for example.

CRediT authorship contribution statement

Nassim Benbara: Conceptualization, Methodology, Software, Validation, Writing – original draft. **Guillaume Martin:** Conceptualization, Methodology, Software, Validation, Writing – review & editing. **Marc Rébillat:** Methodology, Software, Supervision, Writing – review & editing. **Nazih Mechbal:** Funding acquisition, Supervision, Writing – review & editing.

Declaration of competing interest

The authors declare that they have no known competing financial interests or personal relationships that could have appeared to influence the work reported in this paper.

Acknowledgment

References

[1] A.J. Berkhout, D. de Vries, P. Vogel, Acoustic control by wave field synthesis, J. Acoust. Soc. Am. 93 (5) (1993) 2764–2778, http://dx.doi.org/10.1121/1.405852, arXiv:https://doi.org/10.1121/1.405852.

[2] R. Rabenstein, S. Spors, Spatial aliasing artifacts produced by linear and circular loudspeaker arrays used for wave field synthesis, in: Audio Engineering Society Convention, Vol. 120, 2006, URL http://www.aes.org/e-lib/browse.cfm?elib=13515.

[3] N. Harris, M.J. Hawksford, The distributed-mode loudspeaker (DML) as a broad-band acoustic radiator, in: Audio Engineering Society Convention, Vol. 103, 1997, URL http://www.aes.org/e-lib/browse.cfm?elib=7253.

[4] M. Kuster, D. De Vries, D. Beer, S. Brix, Structural and acoustic analysis of multiactuator panels, J. Audio Eng. Soc. 54 (11) (2006) 1065–1076, URL http://www.aes.org/e-lib/browse.cfm?elib=13887.

[5] M. Rébillat, Vibrations of Large Multi-Actuator Panels for the Creation of Audio-Visual Virtual Environments: Acoustical, Mechanical and Perceptual Approaches (Ph.D. thesis), Ecole Polytechnique X, 2011, URL https://pastel.archives-ouvertes.fr/pastel-00657634.

[6] B. Pueo, J.J. López, J. Escolano, L. Hörchens, Multiactuator panels for wave field synthesis: Evolution and present developments, J. Audio Eng. Soc. 58 (12) (2011) 1045–1063, URL http://www.aes.org/e-lib/browse.cfm?elib=15745.

[7] S. Wrona, M. Pawelczyk, X. Qiu, Shaping the acoustic radiation of a vibrating plate, J. Sound Vib. 476 (2020) 115285, http://dx.doi.org/10.1016/j.jsv.2020.115285, URL https://www.sciencedirect.com/science/article/pii/S0022460X20301164.

[8] J. Jung, C.-H. Jeong, J.S. Jensen, Spectrally smooth and spatially uniform sound radiation from a thin plate structure using band gaps, J. Sound Vib. 471 (2020) 115187, http://dx.doi.org/10.1016/j.jsv.2020.115187, URL https://www.sciencedirect.com/science/article/pii/S0022460X20300183.

[9] M.C. Heilemann, D. Anderson, M.F. Bocko, Sound-source localization on flat-panel loudspeakers, J. Audio Eng. Soc. 65 (3) (2017) 168–177, URL http://www.aes.org/e-lib/browse.cfm?elib=18552.

[10] M. Fink, Time reversal of ultrasonic fields. I. Basic principles, IEEE Trans. Ultrason. Ferroelectr. Freq. Control 39 (5) (1992) 555–566, http://dx.doi.org/10.1109/58.156174.

[11] Y. Kahana, P.A. Nelson, O. Kirkeby, H. Hamada, A multiple microphone recording technique for the generation of virtual acoustic images, J. Acoust. Soc. Am. 105 (3) (1999) 1503–1516, http://dx.doi.org/10.1121/1.426690, arXiv:https://doi.org/10.1121/1.426690.

[12] M. Tanter, J.-L. Thomas, M. Fink, Time reversal and the inverse filter, J. Acoust. Soc. Am. 108 (1) (2000) 223–234, http://dx.doi.org/10.1121/1.429459, arXiv:https://doi.org/10.1121/1.429459.

[13] J.-H. Woo, J.-G. Ih, Y. Park, Comparison of two vibro-acoustic inverse methods to radiate a uniform sound field from a plate, J. Sound Vib. 458 (2019) 445–457, http://dx.doi.org/10.1016/j.jsv.2019.06.031, URL http://www.sciencedirect.com/science/article/pii/S0022460X19303700.

[14] K.-H. Lee, J.-G. Ih, A simulation study on the array control of a rectangular panel speaker for improving the sound radiation performance, J. Sound Vib. 488 (2020) 115631, http://dx.doi.org/10.1016/j.jsv.2020.115631, URL http://www.sciencedirect.com/science/article/pii/S0022460X20304624.

[15] K.-H. Lee, J.-G. Ih, D. Jung, A strip speaker using the traveling bending wave on a beam controlled by three actuators, J. Sound Vib. 504 (2021) 116136, http://dx.doi.org/10.1016/j.jsv.2021.116136, URL https://www.sciencedirect.com/science/article/pii/S0022460X2100208X.

[16] J. Woo, J. Ih, Generation of a virtual speaker and baffle on a thin plate controlled by an actuator array at the boundary, IEEE/ASME Trans. Mech. 24 (3) (2019) 1197–1207, http://dx.doi.org/10.1109/TMECH.2019.2906376.

[17] N. Benbara, M. Rebillat, N. Mechbal, Bending waves focusing in arbitrary shaped plate-like structures: Application to spatial audio in cars, J. Sound Vib. 487 (2020) 115587, http://dx.doi.org/10.1016/j.jsv.2020.115587, URL http://www.sciencedirect.com/science/article/pii/S0022460X20304193.

[18] M.L. Manchado, L. Valentini, J. Biagiotti, J. Kenny, Thermal and mechanical properties of single-walled carbon nanotubes–polypropylene composites prepared by melt processing, Carbon 43 (7) (2005) 1499–1505, http://dx.doi.org/10.1016/j.carbon.2005.01.031, URL http://www.sciencedirect.com/science/article/pii/S0008622305000771.

[19] B. Alcock, N. Cabrera, N.-M. Barkoula, C. Reynolds, L. Govaert, T. Peijs, The effect of temperature and strain rate on the mechanical properties of highly oriented polypropylene tapes and all-polypropylene composites, Compos. Sci. Technol. 67 (10) (2007) 2061–2070, http://dx.doi.org/10.1016/j.compscitech.2006.11.012, URL http://www.sciencedirect.com/science/article/pii/S0266353806004465.

[20] S. Pandini, A. Pegoretti, Time and temperature effects on Poisson's ratio of poly(butylene terephthalate), in: Express Polymer Letters, Vol. 5, 2011, pp. 685–697, http://dx.doi.org/10.3144/expresspolymlett.2011.67.

[21] M. Zerrad, R. Rinaldi, B. Eller, N. Totaro, Influence of the micro- and macro-structural parameters on the dynamic behavior of structures made of polymers reinforced with short glass fibers, in: 10th International Styrian Noise, Vibration & Harshness Congress: The European Automotive Noise Conference, Graz, Austria, 2018, http://dx.doi.org/10.4271/2018-01-1501, URL https://hal.archives-ouvertes.fr/hal-01896746.

[22] A. Douglass, J. Harley, Dynamic time warping temperature compensation for guided wave structural health monitoring, IEEE Trans. Ultrason. Ferroelectr. Freq. Control PP (2018) 1, http://dx.doi.org/10.1109/TUFFC.2018.2813278.

[23] C. Fendzi, M. Rébillat, N. Mechbal, M. Guskov, G. Coffignal, A data-driven temperature compensation approach for structural health monitoring using lamb waves, Struct. Health Monit. 15 (5) (2016) 525–540, http://dx.doi.org/10.1177/1475921716650997, arXiv:https://doi.org/10.1177/1475921716650997.

[24] Y. Xia, H. Hao, G. Zanardo, A. Deeks, Long term vibration monitoring of an RC slab: Temperature and humidity effect, Eng. Struct. 28 (3) (2006) 441–452, http://dx.doi.org/10.1016/j.engstruct.2005.09.001, URL http://www.sciencedirect.com/science/article/pii/S0141029605003172.

[25] H. Sohn, M. Dzwonczyk, E.G. Straser, A.S. Kiremidjian, K.H. Law, T. Meng, An experimental study of temperature effect on modal parameters of the alamosa canyon bridge, Earthq. Eng. Struct. Dyn. 28 (8) (1999) 879–897, http://dx.doi.org/10.1002/(SICI)1096-9845(199908)28:8<879::AID-EQE845>3.0.CO;2-V, URL https://onlinelibrary.wiley.com/doi/abs/10.1002/%28SICI%291096-9845%28199908%2928%3A8%3C879%3A%3AAID-EQE845%3E3.0.CO%3B2-V.

[26] B. Peeters, G.D. Roeck, One-year monitoring of the z24-bridge: environmental effects versus damage events, Earthquake Engineering & Structural Dynamics 30 (2) (2001) 149–171, http://dx.doi.org/10.1002/1096-9845(200102)30:2<149::AID-EQE1>3.0.CO;2-Z, URL https://onlinelibrary.wiley.com/doi/abs/10.1002/1096-9845%28200102%2930%3A2%3C149%3A%3AAID-EQE1%3E3.0.CO%3B2-Z.

[27] P. Moser, B. Moaveni, Environmental effects on the identified natural frequencies of the dowling hall footbridge, Mech. Syst. Signal Process. 25 (7) (2011) 2336–2357, http://dx.doi.org/10.1016/j.ymssp.2011.03.005, URL http://www.sciencedirect.com/science/article/pii/S0888327011001233.

[28] B. Moaveni, I. Behmanesh, Effects of changing ambient temperature on finite element model updating of the dowling hall footbridge, Eng. Struct. 43 (2012) 58–68, http://dx.doi.org/10.1016/j.engstruct.2012.05.009, URL http://www.sciencedirect.com/science/article/pii/S0141029612002453.

[29] Y.Q. Ni, X.G. Hua, K.Q. Fan, J.M. Ko, Correlating modal properties with temperature using long-term monitoring data and support vector machine technique, Eng. Struct. 27 (12) (2005) 1762–1773, http://dx.doi.org/10.1016/j.engstruct.2005.02.020, URL http://www.sciencedirect.com/science/article/pii/S0141029605002221.

[30] Y.Q. Ni, H.F. Zhou, J.M. Ko, Generalization capability of neural network models for temperature-frequency correlation using monitoring data, J. Struct. Eng. 135 (10) (2009) 1290–1300, http://dx.doi.org/10.1061/(ASCE)ST.1943-541X.0000050, URL https://ascelibrary.org/doi/abs/10.1061/%28ASCE%29ST.1943-541X.0000050.

[31] H. Li, S. Li, J. Ou, H. Li, Modal identification of bridges under varying environmental conditions: Temperature and wind effects, Struct. Control Health Monit. 17 (5) (2010) 495–512, http://dx.doi.org/10.1002/stc.319, URL https://onlinelibrary.wiley.com/doi/abs/10.1002/stc.319.

[32] H.F. Zhou, Y.Q. Ni, J.M. Ko, Constructing input to neural networks for modeling temperature-caused modal variability: Mean temperatures, effective temperatures, and principal components of temperatures, Eng. Struct. 32 (6) (2010) 1747–1759, http://dx.doi.org/10.1016/j.engstruct.2010.02.026, URL http://www.sciencedirect.com/science/article/pii/S0141029610000799.

[33] W. Shan, X. Wang, Y. Jiao, Modeling of temperature effect on modal frequency of concrete beam based on field monitoring data, 2018, http://dx.doi.org/10.1155/2018/8072843, URL https://www.hindawi.com/journals/sv/2018/8072843/.

[34] J. Jang, A.W. Smyth, Data-driven models for temperature distribution effects on natural frequencies and thermal prestress modeling, Struct. Control Health Monit. 27 (2) (2020) e2489, http://dx.doi.org/10.1002/stc.2489, URL https://onlinelibrary.wiley.com/doi/abs/10.1002/stc.2489.

[35] E. Balmes, M. Corus, D. Siegert, Modeling thermal effects on bridge dynamic responses, 2006.

[36] R. Hou, X. Wang, Q. Xia, Y. Xia, Sparse Bayesian learning for structural damage detection under varying temperature conditions, Mech. Syst. Signal Process. 145 (2020) 106965, http://dx.doi.org/10.1016/j.ymssp.2020.106965, URL http://www.sciencedirect.com/science/article/pii/S0888327020303514.

[37] J.-F. Aubry, M. Tanter, J. Gerber, J.-L. Thomas, M. Fink, Optimal focusing by spatio-temporal inverse filter. II. Experiments. Application to focusing through absorbing and reverberating media, J. Acoust. Soc. Am. 110 (1) (2001) 48–58, http://dx.doi.org/10.1121/1.1377052, arXiv:https://doi.org/10.1121/1.1377052.

[38] C. Hudin, J. Lozada, V. Hayward, Localized tactile feedback on a transparent surface through time-reversal wave focusing, IEEE Trans. Haptics 8 (2) (2015) 188–198, http://dx.doi.org/10.1109/TOH.2015.2411267.

[39] Structural Dynamics Toolbox (for use with MALTAB), SDTools, Paris, France, 1995–2019, https://www.sdtools.com/.

[40] Noliac NCE51 Datasheet, URL http://www.noliac.com/products/materials/nce51/.

[41] D. Ewins, Modal testing: theory and practice, 1984.

[42] A. Simpkins, System identification: Theory for the user, 2nd edition (Ljung, L.; 1999) [on the shelf], IEEE Robot. Autom. Mag. 19 (2) (2012) 95–96, http://dx.doi.org/10.1109/MRA.2012.2192817.

[43] E. Balmes, Frequency domain identification of structural dynamics using the pole/residue parametrization, in: International Modal Analysis Conference, 1996, pp. 540–546.

[44] G. Martin, E. Balmes, T. Chancelier, Characterization of identification errors and uses in localization of poor modal correlation, Mech. Syst. Signal Process. 88 (2017) 62–80, http://dx.doi.org/10.1016/j.ymssp.2016.11.006, URL http://www.sciencedirect.com/science/article/pii/S0888327016304691.

[45] G. Martin, Méthode de Corrélation Calcul/essai Pour L'analyse du Crissement (Ph.D. thesis), Ecole nationale supérieure d'arts et métiers - ENSAM, 2017, URL https://pastel.archives-ouvertes.fr/tel-01553827.

[46] A. Shrivastava, 1 - Introduction to plastics engineering, in: A. Shrivastava (Ed.), Introduction to Plastics Engineering, in: Plastics Design Library, William Andrew Publishing, 2018, pp. 1–16, http://dx.doi.org/10.1016/B978-0-323-39500-7.00001-0, URL https://www.sciencedirect.com/science/article/pii/B9780323395007000010.

[47] M.I. Friswell, J.E. Mottershead, Finite element model updating in structural dynamics, 1995, http://dx.doi.org/10.1007/978-94-015-8508-8.

[48] R. Allemang, The modal assurance criterion - twenty years of use and abuse, J. Sound Vib. 37 (2003) 14–23.

[49] G. Cybenko, Approximation by superpositions of a sigmoidal function, Math. Control Signals Syst. 2 (1989) 303–314.

[50] D.J.C. MacKay, A practical Bayesian framework for backprop networks, Neural Comput. 4 (1992) 448–472.